International Journal of Nanomedicine

Dovepress
open access to scientific and medical research

Open Access Full Text Article

ORIGINAL RESEARCH

Surface Engineering of Metal–Organic Framework as pH-/NIR-Responsive Nanocarrier for Imaging-Guided Chemo-Photothermal Therapy

This article was published in the following Dove Press journal:
International Journal of Nanomedicine

Haibin Guo*
Yanqing Xia*
Ke Feng
Xiaowei Qu
Cuilian Zhang
Feng Wan

Henan Provincial People's Hospital, Henan Provincial Reproductive Hospital, People's Hospital of Zhengzhou University, People's Hospital of Henan University, Zhengzhou, Henan 450003, People's Republic of China

*These authors contributed equally to this work

Background: Metal–organic frameworks (MOFs) have attracted intensive research interest in the biomedical field because of their unique properties. However, in order to realize the high loading capacity and therapeutic efficacy, it is still urgent to develop a multifunctional MOFs-based nanoplatform.

Materials and Methods: Herein, a pH/near-infrared (NIR) dual-responsive drug delivery system based on zeolitic imidazolate framework-8 (ZIF-8) is constructed for synergistic chemo-photothermal therapy and dual-modal magnetic resonance (MR)/photoacoustic (PA) imaging. The doxorubicin hydrochloride (DOX) is embedded into ZIF-8 through one-pot method, and the resultant ZIF-8/DOX is then successively modified with polydopamine, Mn ions and poly(ethylene glycol). The obtained ZIF-8/DMPP is systematically characterized, and both its in vitro and in vivo biological effects are evaluated in detail.

Results: The ZIF-8/DMPP possesses a high drug-loading content of 18.9% and displays appropriate size and morphology. The pH-dependent degradation and drug release behavior of prepared ZIF-8/DMPP are confirmed. Importantly, the results demonstrate that the photothermal effect of ZIF-8/DMPP under NIR laser irradiation can significantly accelerate its drug releasing rate, further improving the intracellular drug concentrations. Thereafter, the augmented chemotherapeutic efficiency by photothermal effect against cancer cells is verified both in vitro and in vivo. Besides, the favorable MR and PA imaging capacity of ZIF-8/DMPP is also evidenced on the tumor model.

Conclusion: Taken together, the surface engineering of ZIF-8-based nanocarrier in this work offers a promising strategy for the multifunctional MOFs-based drug delivery system.

Keywords: zeolitic imidazolate framework-8, pH/NIR responsive, chemo-photothermal therapy, dual-modal imaging

Introduction

Cancer continues to be one of the most threatening killers on human life worldwide.[1] In spite of the flourishing development of varied new therapeutic approaches, chemotherapy still remains to be a mainstay for combating with many kinds of malignancies. Unfortunately, chemotherapeutic drugs in free formation always lead to adverse effects on health tissues and even the immune system.[2] Nanocarriers have been intensively engineered as stimuli-responsive drug delivery systems to load and intelligently release various drug molecules.[3] In order to achieve superior efficacy, the drugs need to be loaded into nanocarriers with high loading content and released at the target site in a controllable and specific-responsive manner. On the other hand, the mere

Correspondence: Feng Wan; Cuilian Zhang
Henan Provincial People's Hospital, Henan Provincial Reproductive Hospital, People's Hospital of Zhengzhou University, People's Hospital of Henan University, Zhengzhou, Henan 450003, People's Republic of China
Tel +86 371 87160762
Email fengwanscholar@163.com; zhangcuilian@henu.edu.cn

submit your manuscript | www.dovepress.com
DovePress
http://doi.org/10.2147/IJN.S239910

chemotherapeutic drug is insufficient to completely kill cancer cells, so it is highly desired to develop a multifunctional nanoplatform for more efficient therapy. In recent years, the combination of photothermal therapy and chemotherapy has been considered as a promising strategy to augment the therapeutic efficiency and lower the side effects.[4] It has been demonstrated that not only the photothermal effect can efficiently ablate tumor via hyperthermia but also the generated heat energy can act as a controllable switch to accelerate the drug release.[5] Generally, the integration of photothermal therapy with stimuli-responsive drug delivery system requires the rational engineering of nanocarriers to realize multiple purposes. Although some photothermal agents, such as gold nanorods,[6] CuS-based nanomaterials[7] and organic conjugated polymers[8,9] have been applied as nanocarriers for simultaneously photothermal therapy and chemotherapeutic drug delivery, these formulations encounter some undesirable shortcomings, including the low drug-loading capacity, the premature drug leakage before reaching the targeted area and the long-term risk due to the poor biodegradability of those materials.[10] Therefore, it urgent to develop novel nanocarrier equipped with high drug loading, favorable biocompatibility and multiple theranostic functions.

At present, the metal–organic framework (MOF) composed of metal center and organic ligands has emerged as a highly promising nanocarrier due to its adjustable compositions and ultrahigh specific surface area as well as intrinsic biodegradability.[11,12] Among those, zinc-based zeolitic imidazolate framework (ZIF) has drawn more and more attention as drug nanocarriers because of their excellent pH-responsive property and high biocompatibility.[13] In particular, ZIF-8 has recently become a research hotspot in the area of nanomedicine.[14–16] However, with regard to drug delivery, the drug molecules are always loaded into ZIF-8 by physical absorption after the formation of ZIF-8, which leads to low loading efficacy and uncontrollable drug release because of the small pore cavity and opening of ZIF-8. Alternatively, the one-pot method can encapsulate various drug or protein molecules into ZIF-8 during the formation of nanoparticles.[17] Zheng et al[18] reported the one-pot synthesis of drug-encapsulated ZIF-8 and demonstrated that the obtained drug-incorporated ZIF-8 displayed high loading efficiency and pH-dependent drug release. Considering the appealing feature of this one-pot method, the construction of multifunctional nanoplatform based on this type of drug-embedded ZIF-8 is worthwhile.[19] Recently, ZIF-8-based multifunctional platforms are constructed by combining with inorganic photothermal agents like CuS,[20] gold nanomaterials[21,22] and Pt nanosheets.[23] However, the long-term hazards of those inorganic nanomaterials are still debated.[24] Thus, the combination of ZIF-8 with organic materials is more preferable for in vivo theranostics.[25–27] Specially, polydopamine (PDA) has been widely utilized as a photothermal agent to construct multifunctional nanoplatforms due to its excellent biocompatibility, biodegradability and photothermal conversion ability.[28] Moreover, the surface modification of PDA also offers more opportunities for further functionalization and even regulation of cell-interfaces behavior.[29] Overall, considering the unique advantages of drug-embedded ZIF-8 and PDA, it is meaningful to fabricate multifunctional ZIF-8-based nanoplatform for more efficient theranostics by rational surface engineering.

To achieve that goal, in this study, the drug-embedded ZIF-8 is prepared and its surface is rationally engineered for pH/NIR dual-responsive drug delivery and imaging-guided synergistic tumor therapy. The chemotherapeutic drug doxorubicin hydrochloride (DOX) is used as a model drug. DOX-embedded ZIF-8 (ZIF-8/DOX) is prepared by one-pot method and directly modified with PDA. Then, the PDA-coated ZIF-8/DOX is further functionalized with Mn ions and poly(ethylene glycol) (PEG). In the obtained nanoplatform (ZIF-8/DMPP), PDA shell can act as a photothermal agent,[30,31] and Mn ions coordinated on PDA are used as contrast agent for magnetic resonance (MR) imaging due to its lower intrinsic toxicity.[32] Moreover, the strong absorption of PDA coating on the NIR region can also be utilized for photoacoustic (PA) imaging.[33] To the best of our knowledge, the simultaneous engineering of PDA and Mn ions onto ZIF-8-based drug delivery system has never been reported before. The ZIF-8/DMPP is first characterized. Its degradation and responsive drug release behavior are also investigated in detail. The impact of the photothermal effect on intracellular drug delivery of ZIF-8/DMPP is inspected. In addition, the dual-modal MR/PA imaging ability of ZIF-8/DMPP is demonstrated in vivo. Last, the synergistic chemo-photothermal therapeutic efficiency of ZIF-8/DMPP is studied both in vitro and in vivo. Therefore, the engineered ZIF-8-based nanoconstruct is expected to be a promising nanocarrier for efficient cancer theranostics.

Materials and Methods

Materials

Zinc nitrate hexahydrate ($Zn(NO_3)_2{\cdot}6H_2O$), 2-methylimidazole (2-MeIM), tris(hydroxymethyl) aminomethane (Tris) and iron chloride hexahydrate ($FeCl_3{\cdot}6H_2O$) were bought from Aladdin Chemistry, Co., Ltd. (Shanghai, China). *N*-(3-Dimethylaminopropyl)-3-ethylcarbodiimide hydrochloride (EDC) and *N*-Hydroxy succinimide (NHS) were purchased from Sinopharm Chemical Reagent Co. Ltd. (Shanghai, China). Dopamine hydrochloride and fluorescein isothiocyanate (FITC) were commercially provided by Sigma-Aldrich Trading Co., Ltd (Shanghai, China). Thiol-terminated polyethylene glycol (PEG-SH, Mw ~5000 Da) and NH_2-PEG-NH_2 (Mw ~2000 Da) was supplied by Yarebio Co., Ltd. (Shanghai, China). Cell Counting Kit-8 (CCK-8) was purchased from Beyotime Institute of Biotechnology. Roswell Park Memorial Institute 1640 (RPMI-1640) medium, fetal bovine serum (FBS), penicillin–streptomycin and trypsin–EDTA were obtained from Yuanxiang medical equipment Co., Ltd., China. Molecular probes Lysotracker Green DND-26 was obtained from Invitrogen (U.S.). Calcein-AM was purchased from Jiangsu KeyGEN Biotech Corp., Ltd. (Nanjing, China). The ultrapure water at resistivity of 18.2 Ω m was used in all experiments. Other reagents were of analytic grade and used without further purification.

Preparation of ZIF-8/DOX Nanoparticles

The DOX-incorporated ZIF-8 nanoparticles were synthesized according to the previously reported protocol.[18] In brief, $Zn(NO_3)_2{\cdot}6H_2O$ was dissolved in 2 mL of ultrapure water. The pH value of the solution was adjusted to ~8 by NaOH aqueous solution, and DOX aqueous solution was quickly added. The mixture was vigorously stirred for 30 sec, followed by dropwise adding 20 mL of 2-MeIM solution (0.2 g/mL). The growth of ZIF-8/DOX was completed in 10 min. Then, the solution was centrifuged to obtain the red precipitates, which was washed repeatedly by water and ethanol to get pure ZIF-8/DOX.

Synthesis of ZIF-8/DMPP

PDA was grown onto ZIF-8/DOX by mussel-inspired chemistry.[34] Typically, 10 mg of ZIF-8/DOX was ultrasonically dispersed in 9 mL of ethanol–water solution, into which 5 mg of dopamine hydrochloride and 5 mg Tris was added in sequence. The mixture was stirred in an open environment for 4 h. The prepared ZIF-8/DPDA was collected and purified with deionized water for several times. For the coordination of Mn ions,[35] 0.2 mL of $MnSO_4$ solution (0.1 M) was slowly added into 10 mL aqueous dispersion of ZIF-8/DPDA (2 mg/mL). After vigorously stirring for 3 h, the Mn-chelated nanoparticles (ZIF-8/DMPDA) were isolated and purified by centrifugation. Next, for surface functionalization of PEG, the obtained ZIF-8/DMPDA was dispersed in Tris buffer (10 mM, pH 8.5) and reacted with 20 mg of PEG-SH (Mw = 2000 Da) for 0.5 h. After that, the PEGylated ZIF-8/DMPDA, denoted as ZIF-8/DMPP, was collected and purified by centrifugation. For comparison, the ZIF-8/MPP was also prepared according to the above protocol except that the DOX solution was replaced with DI water.

For comparison, the drug-free ZIF-8 was also synthesized and modified with PDA. The PDA-coated ZIF-8 was then modified with NH_2-PEG-NH_2 and Mn ions by the same procedure described above. Last, the obtained ZIF-8/MPP was dispersed in ethanol (2 mg/mL) and reacted with FITC at 40 °C for 3 h. The FITC-labelled ZIF-8/MPP was obtained and washed by centrifugation.

Characterization

The morphology of nanoparticles was observed by a JEOL-2100F transmission electronic microscope (TEM, JEOL Ltd., Japan) with an operating voltage of 200 kV. High-angle annular dark-field scanning transmission electron microscopy (HAADF-STEM) imaging and energy-dispersive X-ray spectroscopy (EDX) elemental mapping were performed by FEI Tecnai G2 F20 S-TWIN at 200 kV. Scanning electron microscopy (SEM) studies were performed on a Hitachi S4800 scanning electron microscope. Zeta potential measurement was conducted on the Zetasizer Nano ZS apparatus (Malvern, UK). The X-ray diffraction (XRD) pattern was recorded by a D/MAX-2550PC diffractometer (Rigaku Inc., Japan) with the Cu–Kα radiation at 40 kV and 200 mA. The size distribution was accessed by dynamic light scattering (DLS) using a BI-200SM multi-angle dynamic/static laser scattering instrument (Brookhaven, USA). Ultraviolet−visible (UV-vis) spectrum was carried out on a Lambda 35 UV−vis spectrophotometer (PerkinElmer, USA) at room temperature. The concentrations of Zn and Mn ions were measured by using a NexloN 300X inductive coupling plasma mass spectrum. (ICP-MS, PerkinElmer, Waltham, MA, USA.).

Measurement of Photothermal Effect

To evaluate its photothermal performance, 0.2 mL aqueous dispersion of ZIF-8/DMPP with various concentrations was illuminated by an 808 nm near-infrared (NIR) laser for 5 min. The solution temperature was monitored by a thermocouple thermometer (DT-8891E, Shenzhen Everbest Machinery Industry Co., Ltd., China).

Degradation of ZIF-8/DMPP

ZIF-8/DMPP was dispersed in phosphate buffer solution (PBS) with two pH conditions (pH 5.5 and 7.4). The dispersions were placed in a shaker. At different time points, the dispersions were dropped and dried on a copper grid for TEM observation.

To investigate ions release behavior, the ZIF-8/DMPP was dispersed in 1 mL of PBS (4 mg/mL) with two pH conditions (pH 5.5 and 7.4) and sealed in a dialysis bag (cut-off Mw ~3500 Da). The dialysis bag was then immersed in 9 mL of PBS with the same pH and incubated in a shaker. At predetermined time points, the samples were taken out and the concentrations of Zn and Mn ions were measured by ICP-MS.

In vitro Drug Release

Typically, 1 mL of ZIF-8/DMPP dispersion was sealed in a dialysis bag (cut-off Mw ~3500 Da). Then, the dialysis bag was immersed in 4 mL of PBS (pH 5.5 and 7.4) and incubated in a shaker at 37 °C. One milliliter of releasing media was withdrawn for testing and equivalent fresh media was added back. For photothermal-triggered drug release, the solutions were irradiated by 808 nm NIR laser for 10 min, and the medium was also extracted and subjected to UV-vis spectroscopy. Furthermore, the DOX release experiment was also conducted under the same condition in the absence of NIR laser irradiation.

Cellular Uptake of ZIF-8/DMPP

All cells were purchased from the Chinese Academy of Sciences, Shanghai Institute of Cell Biology (Shanghai, China). Human prostate carcinoma cell line PC-3 and human umbilical vein endothelial cells (HUVECs) were cultured in RPMI-1640 medium supplemented with 10% FBS and 1% penicillin/streptomycin and incubated at 37 °C in 5% CO_2. The medium was changed every 2 days and cells were detached by trypsin-EDTA for cell passage and seeding.

The cellular uptake of ZIF-8/DMPP was inspected by a confocal laser scanning microscope (CLSM). PC-3 cells were seeded in a 20 mm glass-bottom culture dish and incubated overnight. Thereafter, the medium was removed and fresh medium containing free DOX or ZIF-8/DMPP (at DOX concentration 5 μg/mL) was added. The cells were incubated for 1 h, irradiated by NIR laser for 10 min and kept another 1 h incubation. Then, the cells were washed with PBS and fixed by 4% paraformaldehyde. Then, DAPI was used to stain the cell nucleus. The fixed samples were directly observed and imaged by CLSM.

For quantitative test, flow cytometry (FCM) was also performed to determine the mean fluorescence. The cells were seeded on a 6-well plate at a density of 0.3 million cells per well and suffered the same protocol as above, and then the cells were digested by trypsin, filtered through 400 mush grid net, and finally subjected for FCM analysis.

The cellular uptake of drug-free ZIF-8/MPP (Figure S1) was also evaluated by PC-3 cells. The FITC-labelled ZIF-8/MPP was incubated with PC-3 cells in a glass-bottom dish for 1 h. Then, the cells were exposed to NIR laser for 10 min and cultured for another 1 h. The cells were slightly rinsed with PBS and fixed by 4% paraformaldehyde. The cell nucleus was stained with DAPI. Finally, the samples were observed by CLSM.

Therapeutic Efficacy of ZIF-8/DMPP

To investigate the combined therapeutic efficacy of ZIF-8/DMPP, PC-3 cells were cultured in a 96-well plate at a density of 10^4 cells/well and incubated overnight. Then, the cells were incubated with ZIF-8/MPP or ZIF-8/DMPP at different concentrations (50 and 100 μg/mL) for 4 h. After that, the groups of photothermal therapy and combined therapy were subjected to the NIR laser irradiation for 10 min, followed by removing the samples. Then, the cells were cleaned and incubated with fresh medium for another 20 h. Finally, the cell viability was evaluated by CCK-8 assay. The untreated cells were set as control group. For live-dead staining, the cells of different groups were stained with calcein-AM and PI for 15 min and observed by an inverted fluorescence microscope.

The effect of NIR laser on cell viability was also investigated. PC-3 cells were seeded in a 96-well plate. After complete adhesion, the cells were irradiated by 808 nm laser for 10 min at different power density (0.5, 1, 2 W/cm^2). Then, the cells were further incubated for 24 h. The cell viability was evaluated by CCK-8 assay. Moreover, the

PC-3 cells were also incubated with ZIF-8/DOX and free DOX at an equivalent DOX concentration of 5 μg/mL for 4 h. Thereafter, the cells were irradiated with 808 nm laser for 10 min. Then, the cells were washed with PBS and cultured in fresh medium for another 20 h. The cell viability was then measured by CCK-8 assay to compare the difference between NIR laser-treated and untreated group. All quantitative cell experiments are performed with four parallel groups.

The Assessment of Imaging Ability

The in vitro MR imaging ability of ZIF-8/DMPP was assessed in terms of transverse proton relaxation times (T_1) and T_1-weighted imaging of ZIF-8/DMPP dispersion. Typically, ZIF-8/DMPP dispersion with different concentrations was subjected to an NMI20-Analyst NMR analyzing and imaging system (Shanghai Niumag Corp., Shanghai, China) to determine the T_1 value. The instrumental parameters were set as follows: TR/TE = 1000/6 ms, matrix = 256 × 256 mm and section thickness = 0.6 mm. The transverse relaxivity (r_1) was calculated and the T_1-weighted MR imaging was also collected.

Six-week-old healthy male Balb/c nude mice and Balb/c mice were commercially provided by Hunan SJA Laboratory Animal Co., Ltd (Hunan, China) and fostered in kept in filter-topped cages with standard rodent and keep light/dark cycle every 12 h. All the in vivo experiments were carried out in accordance with guidelines of the Care and Use of Laboratory Animals published by Zhenzhou University. The procedure was approved by the Medical Ethics Committee of Henan Provincial People's Hospital (No. SYSZ-LL-2018060301). All effort was made to minimize the suffering of experimental mice during the animal experiment period.

As for in vivo MR imaging, the PC-3 cells were subcutaneously injected into the back of nude mice to establish the xenografted tumor model, into which the suspension of ZIF/DMPP was injected in situ (0.1 mL, 2 mg/mL); then, the T_1-weighed images were collected at 30 min post-injection. To perform in vivo PA imaging, the ZIF/DMPP suspension was also injected into the tumor (0.1 mL, 2 mg/mL) and the PA images of the tumor were acquired on Vevo LAZR photoacoustic imaging system.

In vivo Thermal Imaging

The in vivo thermal imaging was conducted to assess the in vivo photothermal effect of ZIF-8/DMPP. After intratumorally injecting 50 μL of ZIF-8/DMPP, the tumor site was illuminated with an 808 nm laser for 10 min. The thermal images were recorded by an IR camera (TiS55, Fluke, USA) at different time points.

In vivo Antitumor Experiment

To evaluate the in vivo antitumor efficiency, the tumor-bearing mice were randomly divided into four groups (n = 4). The treatment schemes were set as follows: 1) control; 2) ZIF-8/DMPP for chemotherapy only; 3) ZIF-8/MPP + laser for photothermal therapy and 4) ZIF-8/DMPP + laser for photothermal-chemotherapy. Those formulations were intratumorally injected into the tumor site (50 μL, 5 mg/mL). After 0.5 h post-injection, the tumor site of photothermal and photothermal-chemotherapy groups was exposed to NIR laser irradiation for 10 min. The tumor sizes and body weights were recorded every day. Finally, the tumor volume was calculated by the formula V = tumor length×width^2/2 and normalized to a standard value. After the treatments, the tumor was excreted and stained with paraformaldehyde, embedded with paraffin and sliced for hematoxylin–eosin (H&E) staining.

Histological Evaluation

Balb/c mice were used to evaluate the histological toxicity of drug-free ZIF-8/MPP. Typically, the PBS dispersion of ZIF-8/MPP was injected into mice via trail vein at different injected doses (10 and 20 mg/kg). Then, the mice were continuously observed for 1 week. The major organs were excreted after euthanasia, and fixed, embedded, sliced and stained with H&E for histological evaluation.

Statistical Analysis

The quantitative values were presented as mean ± standard deviation (SD). Statistical analysis was performed by using the one-way analysis of variance (ANOVA) with Tukey's post-test. The statistical significance was expressed as *$p < 0.05$ and **$p < 0.01$.

Results and Discussion

Synthesis of ZIF-8/DMPP

The preparation process of theranostic nanoplatform is schematically illustrated in Figure 1, ZIF-8/DOX is first prepared by one-pot method. Then ZIF-8/DOX is modified with PDA shell, onto which Mn ions are subsequently chelated and PEG is grafted to obtain the final product ZIF-8/DMPP. TEM images show that the as-prepared ZIF-8/DOX nanoparticles appear spherical in shape with

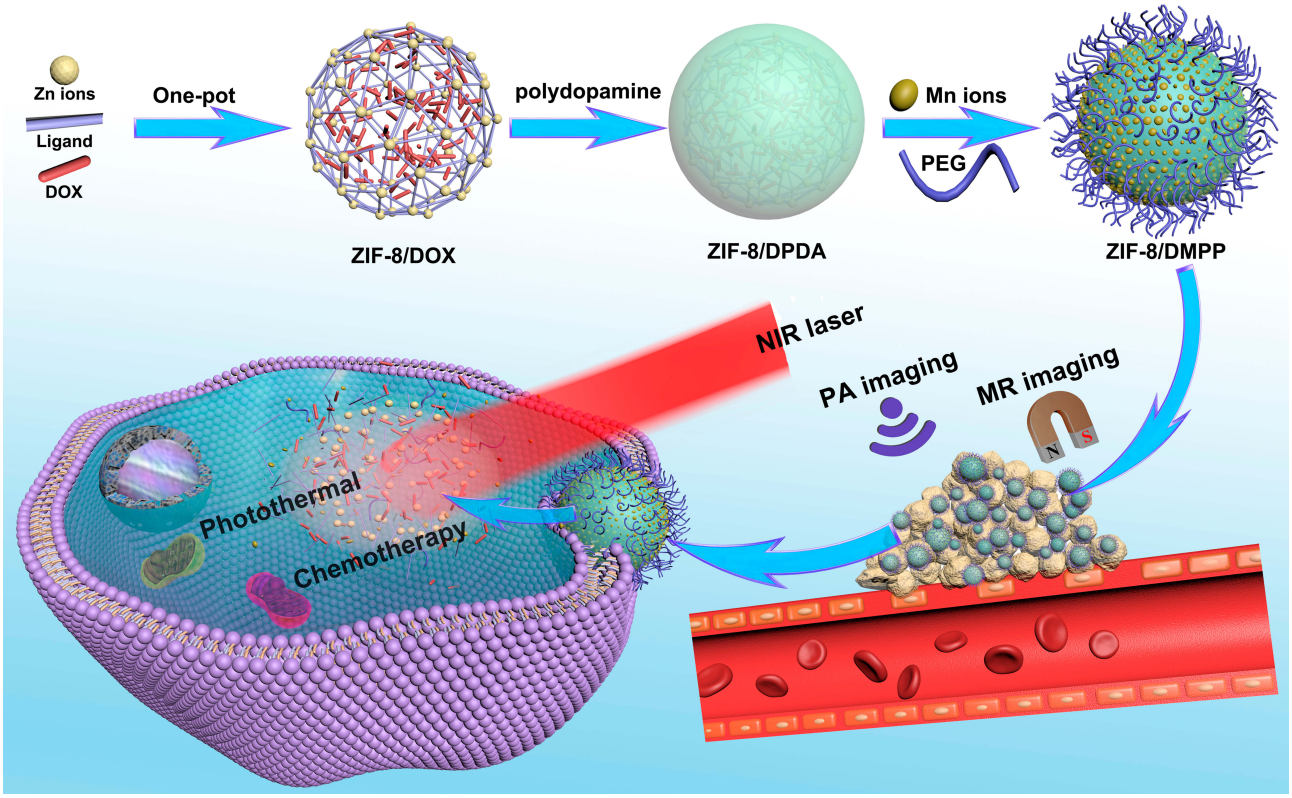

Figure 1 Schematic illustration for the preparation of ZIF-8-based pH/NIR dual-responsive drug delivery system for MR and PA dual-modal imaging-guided chemotherapy.

smooth margin (Figure 2A). After the functionalization, the obtained ZIF-8/DMPP is coated with an organic layer and displays much rough surface (Figure 2B). The apparent difference in morphology between ZIF-8/DOX and ZIF-8/DMPP is clearly evidenced by the inset micrographs with higher magnification. SEM image demonstrates that the obtained ZIF-8/DMPP exhibits good dispersity without significant agglomeration in large field (Figure 2C). The element mapping of STEM image shows that the homogeneous distribution of Zn and C element (Figure 2D). The Mn ions on ZIF-8/DMPP are also confirmed by EDS result (Figure 2E), implying the successful chelation of Mn ions on PDA. Further, the characteristic sharp peaks in XRD pattern indicate that ZIF-8/DOX is highly crystallized. It should be noticed that the surface functionalization on ZIF-8/DOX does not affect its crystal structure since the characteristic peaks are all remained (Figure 2F), which is consistent with previous report.[19] Moreover, DLS data suggests that the hydrodynamic diameter increases from ~206 nm of ZIF-8/DOX to ~272 nm of ZIF-8/DPDA (Figure 2G), verifying successful deposition of PDA coating. The hydrodynamic diameter of ZIF/DMPP also slightly increase due to the chelation of Mn ions and conjugation of PEG. In addition, the surface charge of prepared nanoparticles is measured by zeta potential (Figure 2H). Initially, ZIF-8/DOX is highly positive charged, while ZIF-8/DPDA switches to negative charge because of the abundant phenolic hydroxyl groups of PDA. And the ZIF-8/DMPP also maintains the negative charged surface.[36] The ZIF-8/DMPP can be dispersed in different media without obvious agglomeration and the DLS results also confirm that the size distribution of ZIF-8/DMPP in PBS and cell culture medium is similar with that in water (Figure 2I), indicative of the good colloidal stability of ZIF-8/DMPP.

Photothermal Properties of ZIF-8/DMPP

The obtained ZIF-8/DMPP is also expected to act as excellent photothermal agent due to the existence of PDA shell.[37,38] Accordingly, the photothermal effect of ZIF-8/DMPP is evaluated by monitoring the temperature variation of particle suspensions under NIR laser illumination. As presented in Figure 3A, it can be clearly seen that the temperature of ZIF-8/DMPP suspensions (200 μg/mL) quickly increases 24.3 °C after irradiated by 808 nm laser (2 W/cm^2) for 5 min. In comparison, the temperature of DI

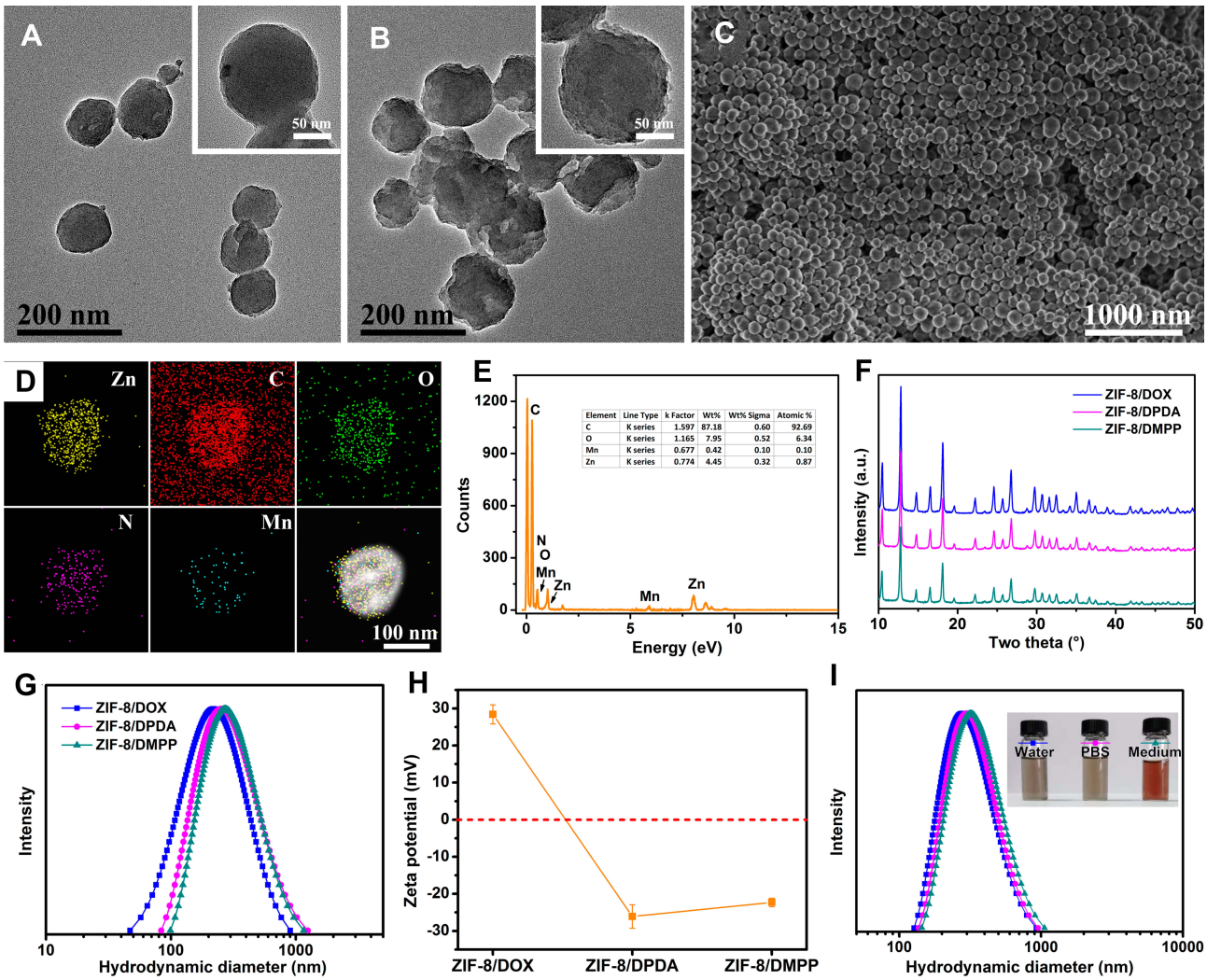

Figure 2 TEM images of (**A**) ZIF-8/DOX and (**B**) ZIF-8/DMPP, inset is the enlarged images. (**C**) SEM images of ZIF-8/DMPP. (**D**) STEM element mapping and (**E**) EDS result of prepared ZIF-8/DMPP. (**F**) XRD pattern. (**G**) DLS size distribution and (**H**) zeta potential results of ZIF-8/DOX, ZIF-8/DPDA and ZIF-8/DMPP. (**I**) DLS size distribution of ZIF-8/DMPP dispersed in different media.

water under same treatment only changes ~2.4 °C, implying NIR laser alone could not arouse satisfied photothermal effect. Figure 3B also shows that the temperature of suspensions elevates correspondingly with the increasing concentration of ZIF-8/DMPP. Thus, the results suggest that the prepared ZIF-8/DMPP possesses good photothermal efficacy.

Drug Release of ZIF-8/DMPP

Next, the DOX release behavior of ZIF-8/DMPP is studied. Actually, it is recognized that the chemotherapeutic drug DOX is almost "locked" into the framework of ZIF-8 during its crystal growth based on the previously reported one-pot method.[39] The distinct absorption peak of DOX is observed in the spectrum of ZIF-8/DOX and dramatically weakened in DOX@HMONs-PDA (Figure S2), which was probably due to the quenching effect of PDA.[40] Moreover, the supernatant solution of ZIF-8/DMPP shows no absorption peaks, indicating the DOX is effectively sealed in the framework. Meanwhile, a high drug-loading content of 18.9% is obtained by this one-pot method. As for drug release, it is expected that the drug release from ZIF-8/DOX is associated with the framework stability of ZIF-8. Not surprisingly, the release rate at pH 5.5 is much faster than that at pH 7.4 (Figure 3C). Over 30% of DOX is released after 1 day for pH 5.5, while less than 5% is released under pH 7.4 at the same time. The faster release at pH 5.5 is probably due to the decomposition of ZIF-8/DMPP under acidic condition. On the other hand, the photothermal effect of the PDA shell on ZIF-8/

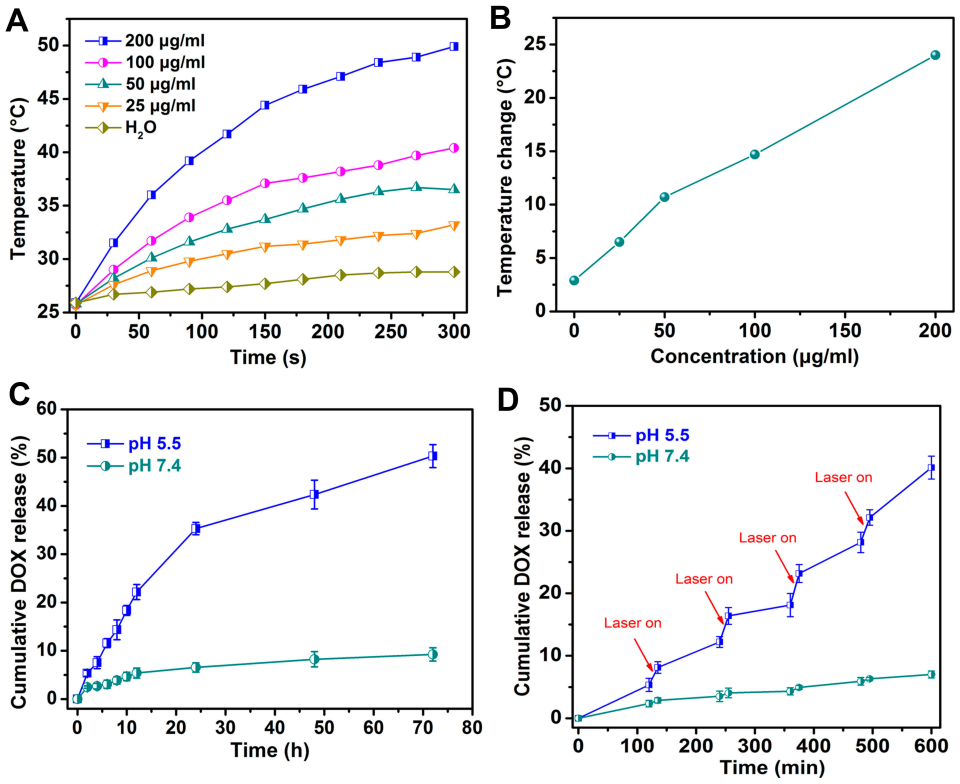

Figure 3 (**A**) The temperature changing curve and (**B**) value of different concentrated ZIF-8/DMPP suspensions exposed to NIR laser for 10 min. (**C**) Cumulative release curve of DOX from ZIF-8/DMPP under different pH conditions. (**D**) The DOX releasing curve of ZIF-8/DMPP under different pH conditions with NIR laser irradiation.

DOX can also accelerate the drug release under laser irradiation.[41] To verify the above descriptions, the releasing experiment at different pH conditions is performed with or without NIR laser irradiation, the results are presented in Figure 3D. As expected, the DOX is released very slow at neutral conditions, in which only 7.0% drugs are released at pH 7.4 even though the NIR laser irradiation is applied. On the contrary, the DOX release at acidic condition is much faster. The data show that the release amount of DOX quickly reaches 12% in the first 4 h. Especially, the release amount of DOX is significantly improved under the NIR laser irradiation. Apparently, the tendency of drug release is in accordance with the degradation behavior of ZIF-8/DMPP. The faster release of DOX under acidic condition can be ascribed to the framework decomposition of ZIF-8/DMPP, while more stable at pH 7.4 resulted in much slower drug diffusion. On the basis of the above results, it is concluded that the drug release behavior of ZIF-8/DMPP is pH-dependent and can be accelerated by NIR laser, which is conducive to combined chemo-photothermal therapy.[42]

Degradation Ability of ZIF-8/DMPP

The degradation property of nanomaterials is of great significance for their biomedical applications. Given the fact that ZIF-8 possesses the intrinsic pH-sensitive degradation behavior,[43] the degradation of the prepared ZIF-8/DMPP is inspected. ZIF-8/DMPP is dispersed in PBS with two different pH values that simulate the physiological and tumor conditions, respectively. As shown in Figure 4A, the morphology of ZIF-8/DMPP incubated at pH 7.4 appears no change even time is prolonged to 6 h, implying its favorable stability under physiological condition. In sharp contrast, the rapid degradation is observed under pH 5.5. The ZIF-8/DMPP displays obvious framework disintegration at 0.5 h, and its intact morphology is almost invisible at 2 h. Finally, only small fragments are observed after 6 h incubation. Clearly, the direct observation in TEM suggests that the prepared ZIF-8/DMPP is stable in neutral conditions and degraded under acidic conditions. Moreover, the result of ions release experiment also demonstrates the degradation of ZIF-8/DMPP. As shown in Figure 4B, Zn ions are rapidly released at pH 5.5,

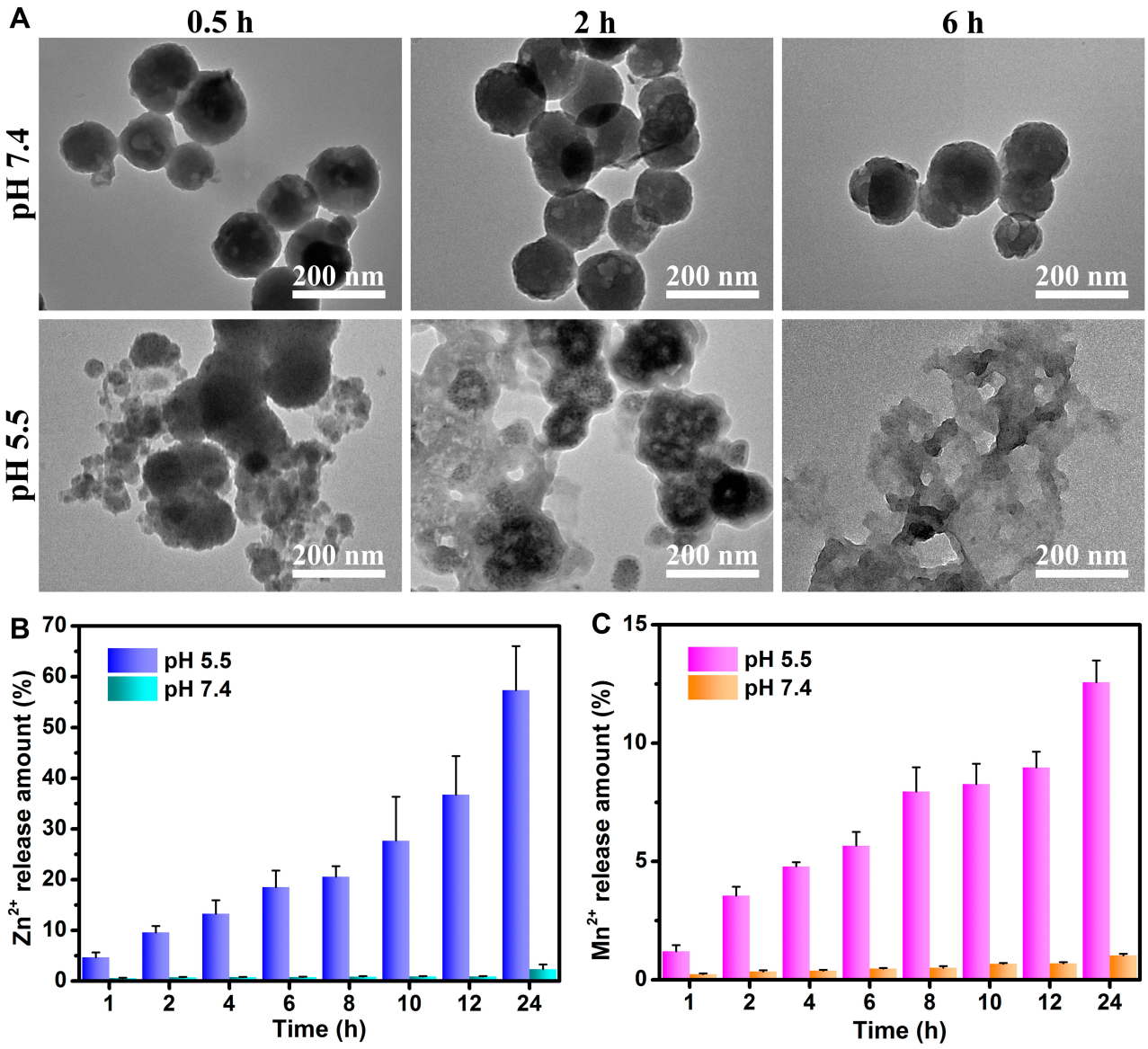

Figure 4 (**A**) TEM images of ZIF-8/DMPP after incubated at pH 7.4 and 5.5 for different time points. Cumulative release of (**B**) Zn^{2+} ions and (**C**) Mn^{2+} ions from ZIF-8/DMPP after incubated at pH 7.4 and 5.5 for different time points.

implying the dissociation of ZIF-8/DMPP under acidic condition. In contrast, the release content of Zn ions is very low at pH 7.4 due to the intact structure of ZIF-8/DMPP under neural condition, which is consistent with the TEM observation. Besides, the same tendency is also observed for the group of Mn ions (Figure 4C). Therefore, those results forcefully confirm the pH-responsive degradation of ZIF-8/DMPP.

Intracellular Drug Delivery of ZIF-8/DMPP

With the appropriate releasing behavior in simulated condition, the intracellular delivering ability of ZIF-8/DMPP is studied by a confocal laser scanning microscope (CLSM). PC-3 cells are incubated with ZIF/DMPP and the CLSM images are presented in Figure 5A. The blue fluorescence of DAPI is surrounded by red fluorescence of DOX, which suggests that ZIF/DMPP can efficiently deliver DOX into cancer cells. More importantly, the red fluorescence in PC-3 cells exposed to NIR laser irradiation is much stronger than that of untreated cells. FCM results also indicate that the peak of DOX fluorescence of ZIF-8/DMPP plus laser irradiation was distinctly right-shifted in comparison to the ZIF-8/DMPP-treated alone (Figure 5B). Besides, the mean fluorescence of ZIF-8/DMPP + laser irradiation is both higher than that of ZIF-8/DMPP alone,

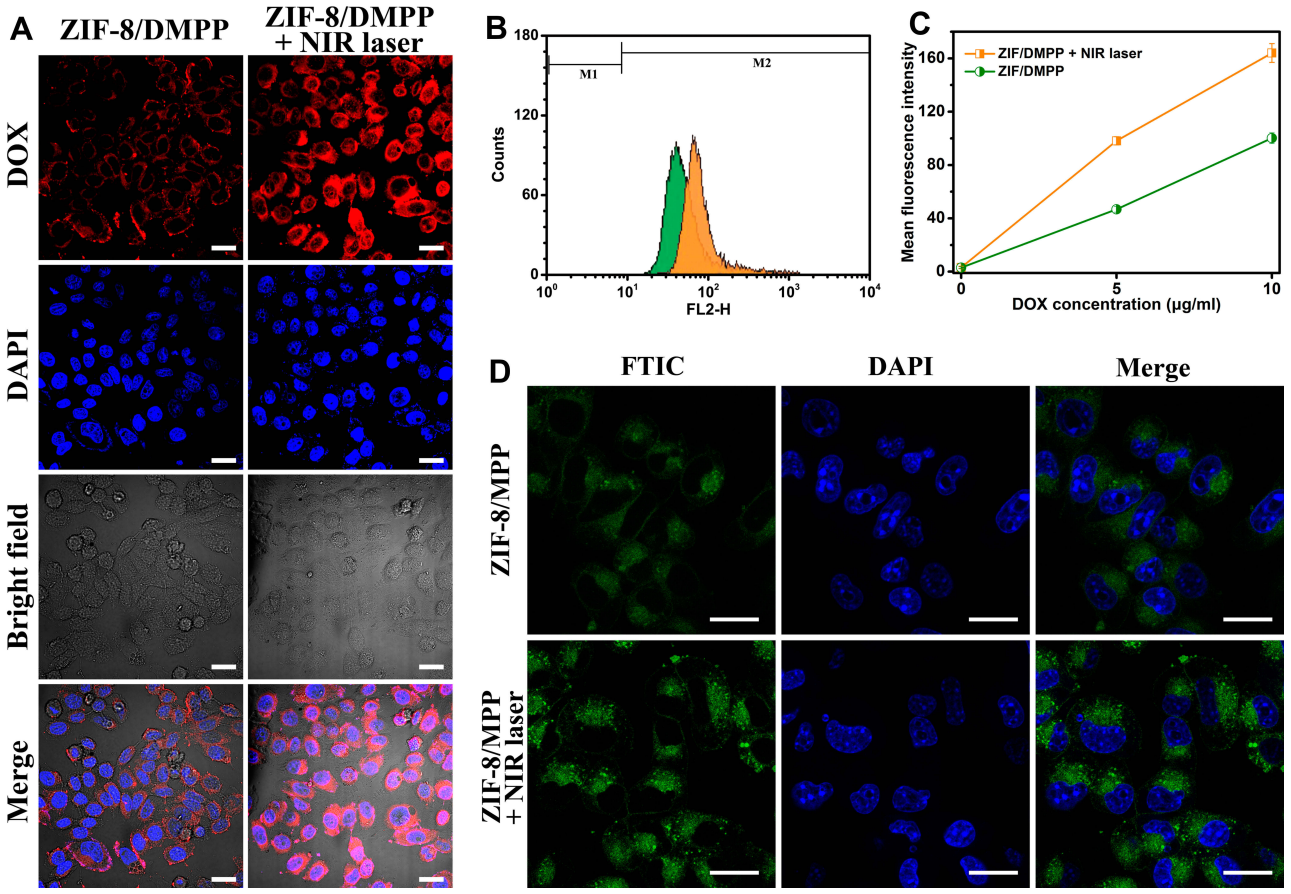

Figure 5 (**A**) Confocal laser scanning microscope (CLSM) images and (**B**) The flow cytometry results and (**C**) mean intracellular fluorescent intensity of PC-3 cells treated by ZIF-8/DMPP with or without NIR laser irradiation. (**D**) CLSM images of PC-3 cells incubated with FITC-labelled drug-free ZIF-8/MPP for 2 h with or without NIR laser irradiation. Scale bar in (**A**) and (**D**) is 20 μm.

regardless of the drug concentration (Figure 5C). This result demonstrates that the NIR laser irradiation can greatly improve the intracellular delivery of ZIF-8/DMPP. The photothermal effect of ZIF-8/DMPP is attributed to this through two major aspects: on one hand, the elevated temperature could enhance the permeability of cancer cell membranes,[10,44] making more particles being internalized into cells; on the other hand, the thermal effect also promotes the drug diffusion from ZIF-8/DMPP as mentioned above. To further demonstrate the photothermal enhanced cellular uptake, the drug-free ZIF-8/MPP is labelled with FITC and incubated with PC-3 cells under NIR laser irradiation. The CLSM images show that the green fluorescence of NIR laser-treated group is obviously stronger than that of untreated cells (Figure 5D). The fluorescent intensity of NIR laser-treated group is also determined to be higher than that of mere ZIF-8/DMPP-treated group (Figure S3). Therefore, the NIR laser enhanced drug delivery, together with the aforementioned pH-responsive drug release, is very beneficial for combined chemo-photothermal therapy.[45]

In vitro Combined Chemo-Photothermal Therapy

The in vitro killing effect on PC-3 cells is performed to evaluate the in vitro therapeutic efficiency. First, to exclude the influence of NIR laser alone on cell viability, the 4T1 cells are exposed to 808 nm laser at different power density. The results of CCK-8 assay and live-dead staining indicate that no obvious cell death was detected regardless of power density (Figures 6A and S4), implying that the 808 nm NIR laser alone would not damage the cells. Moreover, the toxicity of free DOX and ZIF-8/DOX is also evaluated both in the presence and absence of NIR laser. Figure 6B shows that both free DOX and ZIF-8/DOX exhibited a similar mortality rate no, matter the NIR laser irradiation is applied or not. Moreover, it should be noticed that the killing effect of ZIF-8/DOX is better than

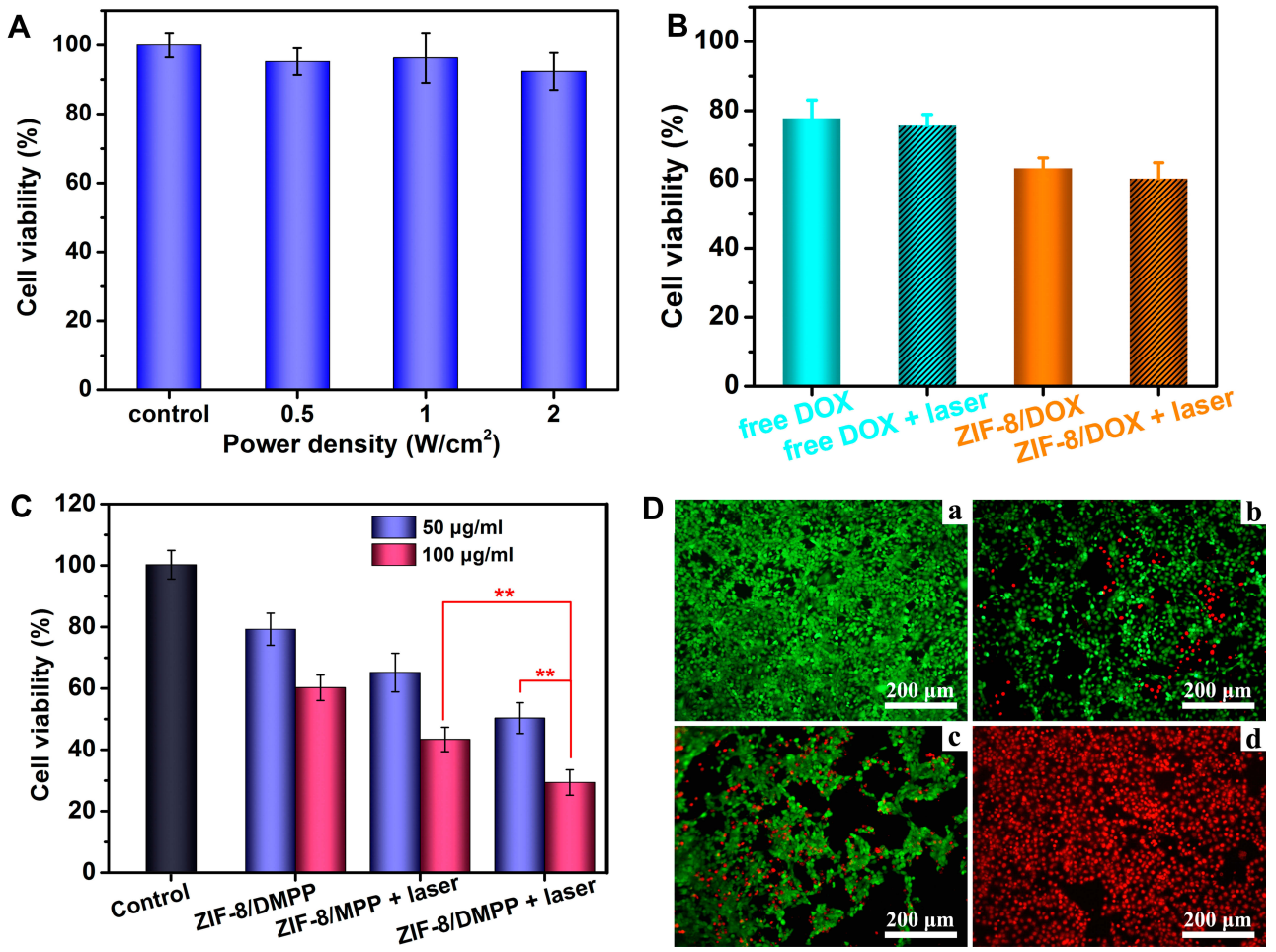

Figure 6 (**A**) Cell viability of PC-3 cells exposed to NIR laser for 10 min at different power density. (**B**) Cell viability of PC-3 cells treated with free DOX or ZIF-8/DOX under normal condition or NIR laser irradiation. (**C**) Cell viability of PC-3 cells after subjected to different treatments. Four parallel experiments were conducted for cell experiments. **Indicates significance with $p < 0.01$. (**D**) The fluorescent images stained by calcein–AM/PI after (a) cell medium, (b) ZIF-8/DMPP, (c) ZIF-8/MPP + laser and (d) ZIF-8/DMPP + laser.

free DOX at the same conditions. It can be attributed to the enhanced intracellular uptake of ZIF-8/DOX because of its strong positive surface. Along with the sustained DOX release from ZIF-8/DOX under acidic intracellular condition, the ZIF-8/DOX can realize improved efficacy toward cancer cells. Therefore, we conclude that the NIR laser alone cannot damage cancer cells.

Next, the cytotoxicity of ZIF-8/MPP is also studied, and the results manifest that no obvious toxicity is detected for both PC-3 cells and HUVECs in studied concentrations (Figure S5). For in vitro therapy, ZIF-8/DMPP, ZIF-8/MPP + laser and ZIF-8/DMPP + laser are set as chemotherapy group, photothermal group and combined therapy group, respectively. As expected, the cell viability exhibits distinct difference after the designated treatments. The ZIF-8/DMPP + laser shows the best killing efficiency of PC-3 cells among those groups. Especially, the death rate of cells treated by ZIF-8/DMPP + laser (100 μg/mL) is as high as 67.64%, while the therapeutic efficacy for single ZIF-8/DMPP or ZIF-8/MPP + laser is only 34.79% and 53.64% (Figure 6C). This result demonstrates the synergistic effects of combined chemo-photothermal therapy, which is resulted from the photothermal effect itself and the photothermal improved intracellular drug concentration as proven above.

To visualize the therapeutic effect of different groups, the live-dead cell staining is also performed. As shown in Figure 6D, the cells of control group are all stained with green fluorescence of Calcein–AM. In contrast, the red spots of PI for combined therapy are much more than single therapy. Together, it is confirmed that the prepared ZIF-8/DMPP can exert an excellent synergistic effect to efficiently kill cancer cells.

The Dual-Modal Imaging of ZIF-8/DMPP

The Mn ions chelated on ZIF-8/DMPP can act as a contrast agent for MR imaging. To explore its function, the ZIF-8/DMPP suspensions are diluted into four different concentrations for MR scanning using a scanner with a magnetic field of 0.5 T. The relaxation times of each concentration were recorded and its reciprocal is plotted as a function of ion concentration. Then, the relaxation rate (r_1) is calculated to be 6.03 $mM^{-1}·s^{-1}$. The concentration-dependent brightening ability of the ZIF-8/DMPP suspensions is also observed (Figure 7A), suggesting its good T_1-weighted MR imaging ability. Further, the in vivo MR imaging is also conducted on tumor-bearing mice. Remarkably, the tumor region injected with ZIF-8/DMPP is much brighter than control group (Figure 7B). The result indicates that the ZIF-8/DMPP can be applied as a good contrast agent for in vivo MR imaging.

Furthermore, the strong absorption of PDA in NIR region makes ZIF-8/DMPP possible for PA imaging. Then, in vivo PA imaging is also carried out. Likewise, the PA signals in the tumor region are clearly stronger after injection of ZIF-8/DMPP (Figure 7C), which demonstrates the PA imaging ability of the prepared nanocomposites. Therefore, the chelation of Mn ions onto the PDA shell of ZIF-8/DMPP makes it a potential imaging agent for dual-modal imaging, which is possibly conducive for cancer theranostics.

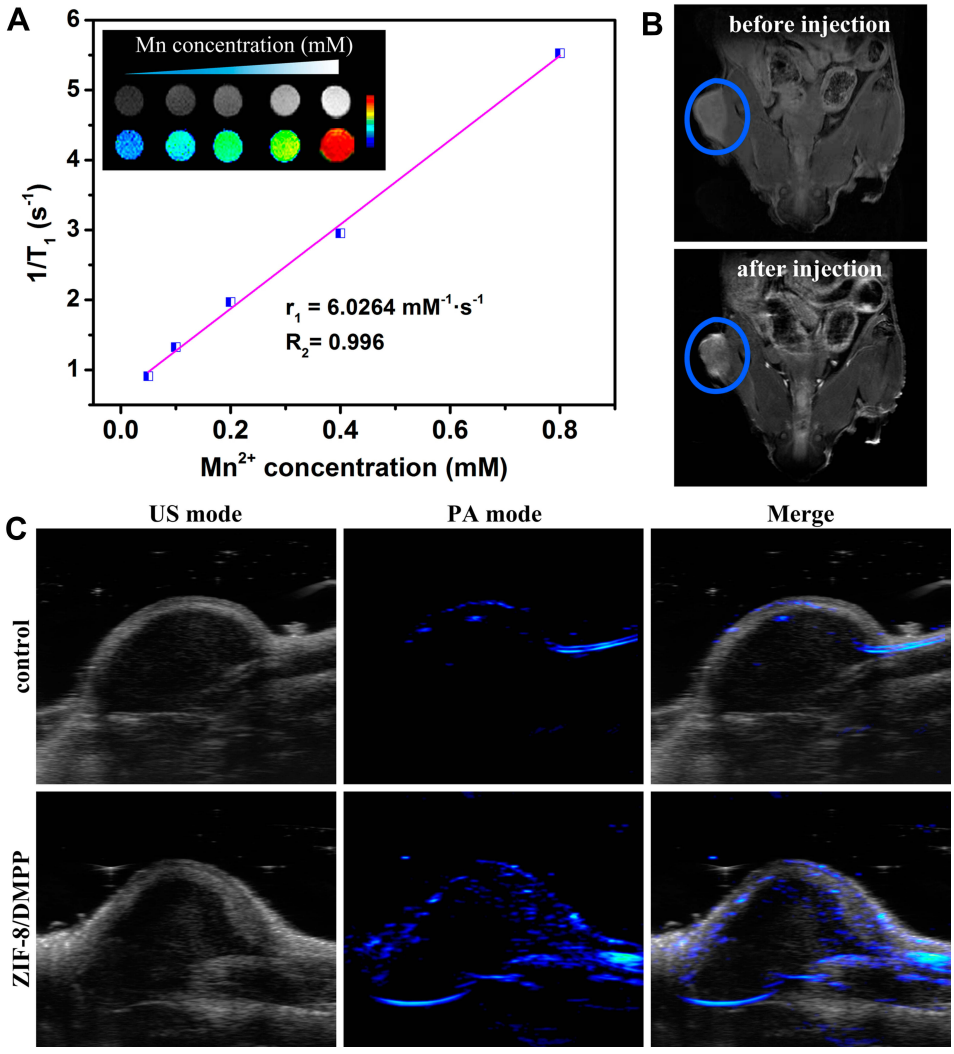

Figure 7 (**A**) T_1 relaxation rates (r_1) and in vitro T_1-weighted MR images of ZIF-8/DMPP at different concentrations. (**B**) In vivo T_1-weighted MR images of tumor-bearing mise injected with or without ZIF-8/DMPP suspensions. The tumor regions are pointed out in the blue circle. (**C**) In vivo PA images of tumor site injected with or without ZIF-8/DMPP suspensions.

In vivo Combined Chemo-Photothermal Therapy

After confirming the in vitro therapeutic efficiency and imaging ability of ZIF-8/DMPP, the tumor-bearing mice are utilized to assess its in vivo antitumor effect. The in vivo photothermal effect of ZIF-8/DMPP is determined first. Figure 8A shows the thermal images of tumor-bearing mice after injection of PBS or ZIF-8/DMPP suspension and exposed to NIR laser (2 W/cm^2). The NIR laser alone cannot induce the thermal effect as the temperature change for control group is only 4.1 °C (Figure 8B). However, the temperature of tumor region injected with ZIF-8/DMPP quickly reach up to 47.5 °C after 10 min irradiation, indicating the good in vivo photothermal effect of ZIF-8/DMPP. After the treatments, the change of tumor volume is calculated and plotted as function of time to compare the antitumor efficiency. The tumor growth of control group is much faster than other groups. It is also noticed that the combined therapy group (ZIF/8-DMPP + laser) exhibits the best inhibition rate as compared to the single therapy. At the end of time period, the normalized tumor volume of ZIF-8/DMPP + laser is as low as 0.17. Despite the photothermal effect can damage the tumor tissue, the long-term inhibition effect is very limited as evidenced by the re-growth tendency in the curve (Figure 8C). As for combined therapy, the photothermal effect and sustained local drug release could efficiently suppress and eliminate the tumor, which is affirmed by both the images of excreted tumor tissue and H&E staining sections (Figure 8E). In particular, a large area of cell fragments and necrosis appears in the combined therapy group as compared with other groups. The body weight of experimental mice is also monitored (Figure 8D). No abnormal situation is found in the whole treatment period, demonstrating that the ZIF-8/DMPP has good biocompatibility and the treatments were well tolerated by mice. Overall, those results illustrate that the ZIF-8/DMPP can effectively conquer the tumor growth in vivo.

In addition, the histocompatibility of the developed nanoplatform is also evaluated. After intravenous injection of drug-free ZIF-8/MPP, the major organs of mice are sliced and stained with H&E. The microscope images suggest that no obvious organ damage or inflammatory response is detected after the injection of different doses of ZIF-8/MPP (Figure 9). Thus, the developed ZIF-8-based nanoplatform possesses excellent histocompatibility for future in vivo applications.

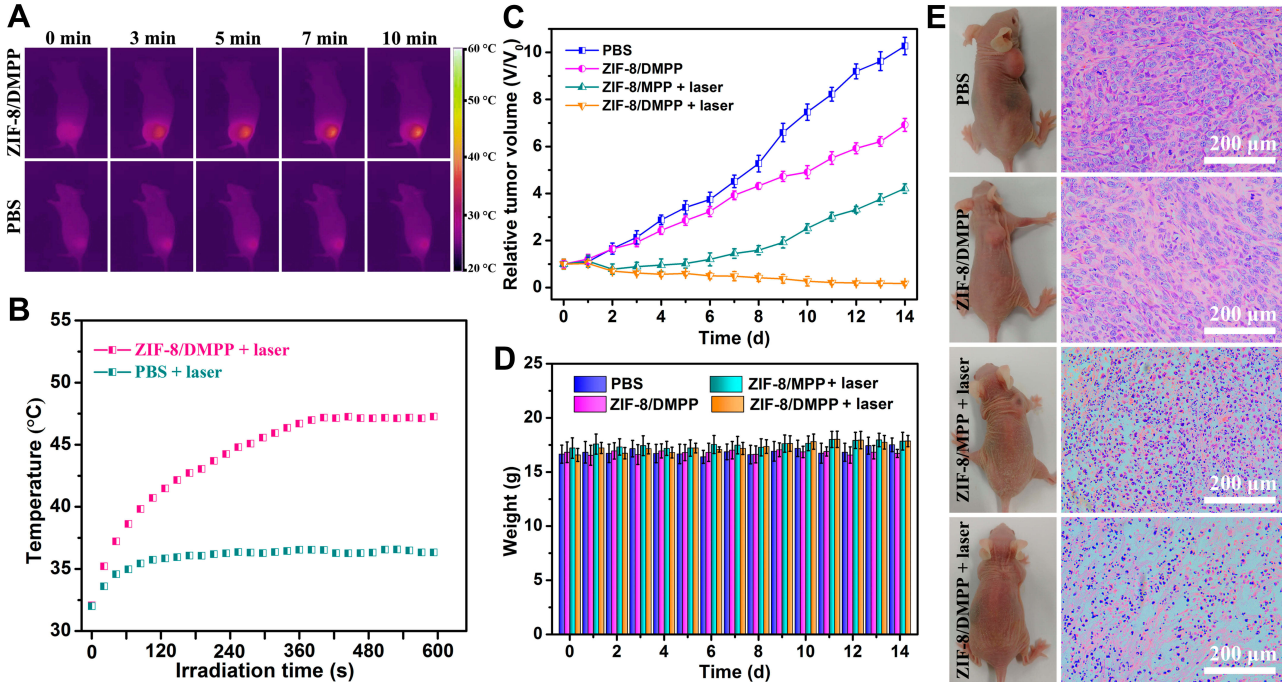

Figure 8 (**A**) Infrared thermal images and (**B**) the highest temperature change of tumor-bearing mice injected with PBS or ZIF-8/DMPP under illumination of NIR laser at different time points. (**C**) The change of relative tumor volume and (**D**) body weight of experiment mice at the treatment duration. (**E**) Represented photos of tumor-bearing mice (left) and H&E staining of the tumor section after the treatments (right).

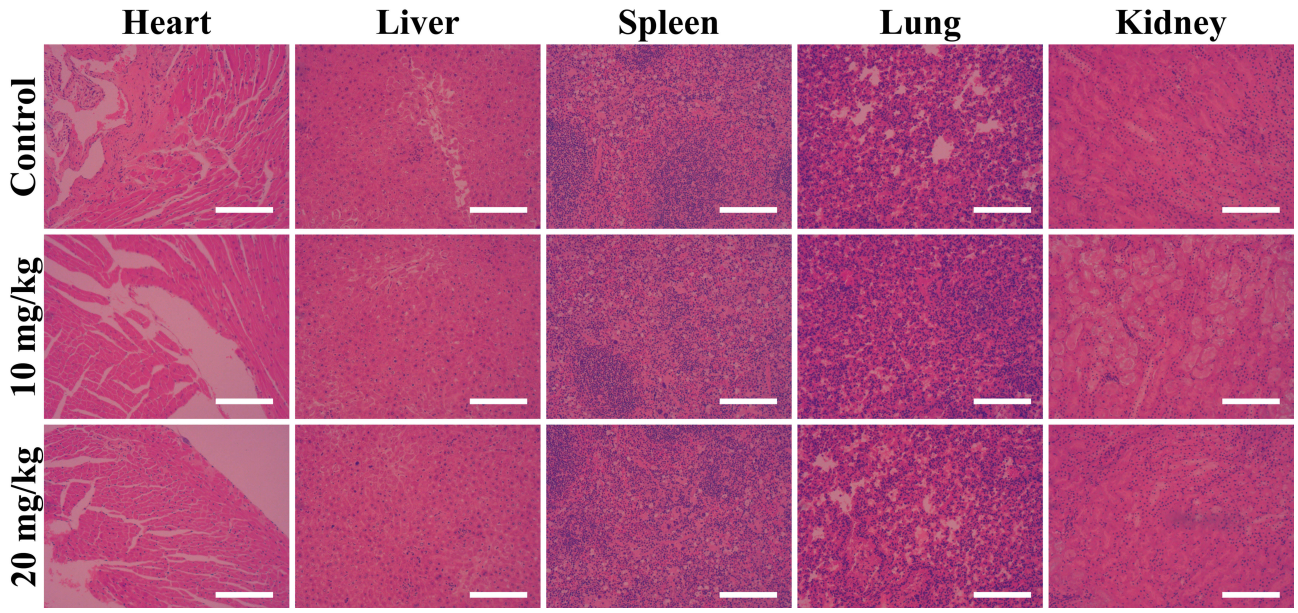

Figure 9 The H&E-stained histological images of major organs of mice injected with ZIF-8/MPP at different doses. The scale bar is 200 μm.

Conclusion

In summary, DOX-embedded ZIF-8 is prepared and functionalized as a smart drug delivery system for combined chemo-photothermal therapy and dual-modal imaging of tumor. ZIF-8/DOX synthesized by one-pot approach achieves high loading of chemotherapeutic drug DOX. The modification of PDA not only renders the resultant nanoconstruct with good photothermal effect but also facilitates its further surface functionalization with Mn ions and PEG. The ZIF-8/DMPP exhibits desirable degradation behavior and sensitive pH-dependent drug release. Meanwhile, the data demonstrate that the photothermal effect of ZIF-8/DMPP could also accelerate the drug release rate, thereby making ZIF-8/DMPP a smart pH/NIR dual-responsive drug delivery system. More importantly, it is also affirmed that the photothermal effect could significantly enhance the cellular uptake of ZIF-8/DMPP. As a consequence, the intracellular drug concentration is improved and the therapeutic efficiency is augmented due to the synergistic effect. In addition, both the T_1-weighted MR imaging and PA imaging capacities are demonstrated in vivo. The in vivo antitumor experiment also suggests the excellent therapeutic efficiency of ZIF-8/DMPP under laser irradiation. Taken together, the presented data manifest that the developed MOFs-based nanoconstruct holds great potential for smart drug delivery and cancer theranostics.

Acknowledgments

This work was financially supported by the Science and Technology Department of Henan Province (142102310393). Haibin Guo and Yanqing Xia are co-first authors for this study.

Disclosure

The authors report no conflicts of interest in this work.

References

1. Shi JJ, Kantoff PW, Wooster R, Farokhzad OC. Cancer nanomedicine: progress, challenges and opportunities. *Nat Rev Cancer*. 2017;17(1):20–37. doi:10.1038/nrc.2016.108
2. Marques MRC, Choo Q, Ashtikar M, Rocha TC, Bremer-Hoffmann S, Wacker MG. Nanomedicines-tiny particles and big challenges. *Adv Drug Deliv Rev*. 2019;151–152:23–43. doi:10.1016/j.addr.2019.06.003
3. Du JZ, Lane LA, Nie SM. Stimuli-responsive nanoparticles for targeting the tumor microenvironment. *J Control Release*. 2015;219:205–214. doi:10.1016/j.jconrel.2015.08.050
4. Meng ZQ, Wei F, Wang RH, et al. NIR-laser-switched in vivo smart nanocapsules for synergic photothermal and chemotherapy of tumors. *Adv Mater*. 2016;28(2):245–253. doi:10.1002/adma.201502669
5. Sun XQ, Wang C, Gao M, Hu AY, Liu Z. Remotely controlled red blood cell carriers for cancer targeting and near-infrared light-triggered drug release in combined photothermal-chemotherapy. *Adv Funct Mater*. 2015;25(16):2386–2394. doi:10.1002/adfm.201500061
6. Zhang N, Xu XF, Zhang X, et al. Nanocomposite hydrogel incorporating gold nanorods and paclitaxel-loaded chitosan micelles for combination photothermal-chemotherapy. *Int J Pharmaceut*. 2016;497(1–2):210–221. doi:10.1016/j.ijpharm.2015.11.032
7. Su XJ, Zhao FF, Wang YH, Yan XS, Jia SN, Du B. CuS as a gatekeeper of mesoporous upconversion nanoparticles-based drug controlled release system for tumor-targeted multimodal imaging and synergetic chemo-thermotherapy. *Nanomedicine (N Y, U S)*. 2017;13(5):1761–1772.

8. Wang C, Xu H, Liang C, et al. Iron oxide @polypyrrole nanoparticles as a multifunctional drug carrier for remotely controlled cancer therapy with synergistic antitumor effect. *ACS Nano*. 2013;7(8):6782–6795. doi:10.1021/nn4017179
9. Xia B, Wang B, Shi JS, et al. Photothermal and biodegradable polyaniline/porous silicon hybrid nanocomposites as drug carriers for combined chemo-photothermal therapy of cancer. *Acta Biomater*. 2017;51:197–208. doi:10.1016/j.actbio.2017.01.015
10. Lu N, Huang P, Fan WP, et al. Tri-stimuli-responsive biodegradable theranostics for mild hyperthermia enhanced chemotherapy. *Biomaterials*. 2017;126:39–48. doi:10.1016/j.biomaterials.2017.02.025
11. Cai W, Wang JQ, Chu CC, Chen W, Wu CS, Liu G. Metal organic framework-based stimuli-responsive systems for drug delivery. *Adv Sci*. 2019;6(1):201801526. doi:10.1002/advs.201801526
12. Rojas S, Arenas-Vivo A, Horcajada P. Metal-organic frameworks: a novel platform for combined advanced therapies. *Coordin Chem Rev*. 2019;388:202–226. doi:10.1016/j.ccr.2019.02.032
13. Wuttke S, Zimpel A, Bein T, et al. Validating metal-organic framework nanoparticles for their nanosafety in diverse biomedical applications. *Adv Healthc Mater*. 2017;6(2):201600818.
14. Sun CY, Qin C, Wang XL, et al. Zeolitic imidazolate framework-8 as efficient pH-sensitive drug delivery vehicle. *Dalton T*. 2012;41(23):6906–6909. doi:10.1039/c2dt30357d
15. Yang K, Yang K, Chao S, Wen J, Pei YX, Pei ZC. A supramolecular hybrid material constructed from pillar[6]arene-based host-guest complexation and ZIF-8 for targeted drug delivery. *Chem Commun*. 2018;54(70):9817–9820. doi:10.1039/C8CC05665J
16. Chen TT, Yi JT, Zhao YY, Chu X. Biomineralized metal-organic framework nanoparticles enable intracellular delivery and endo-lysosomal release of native active proteins. *J Am Chem Soc*. 2018;140(31):9912–9920. doi:10.1021/jacs.8b04457
17. Zhuang J, Kuo CH, Chou LY, Liu DY, Weerapana E, Tsung CK. Optimized metal-organic-framework nanospheres for drug delivery: evaluation of small-molecule encapsulation. *ACS Nano*. 2014;8(3):2812–2819. doi:10.1021/nn406590q
18. Zheng HQ, Zhang YN, Liu LF, et al. One-pot synthesis of metal organic frameworks with encapsulated target molecules and their applications for controlled drug delivery. *J Am Chem Soc*. 2016;138(3):962–968. doi:10.1021/jacs.5b11720
19. Wu Q, Niu M, Chen XW, et al. Biocompatible and biodegradable zeolitic imidazolate framework/polydopamine nanocarriers for dual stimulus triggered tumor thermo-chemotherapy. *Biomaterials*. 2018;162:132–143. doi:10.1016/j.biomaterials.2018.02.022
20. Jiang W, Zhang HY, Wu JL, et al. CuS@MOF-based well-designed quercetin delivery system for chemo-photothermal therapy. *ACS Appl Mater Inter*. 2018;10(40):34513–34523. doi:10.1021/acsami.8b13487
21. Li YT, Jin J, Wang DW, et al. Coordination-responsive drug release inside gold nanorod@metal-organic framework core-shell nanostructures for near-infrared-induced synergistic chemo-photothermal therapy. *Nano Res*. 2018;11(6):3294–3305. doi:10.1007/s12274-017-1874-y
22. Deng XR, Liang S, Cai XC, et al. Yolk-shell structured au nanostar@metal-organic framework for synergistic chemo-photothermal therapy in the second near-infrared window. *Nano Lett*. 2019;19(10):6772–6780. doi:10.1021/acs.nanolett.9b01716
23. Zhu W, Chen M, Liu Y, et al. A dual factor activated metal-organic framework hybrid nanoplatform for photoacoustic imaging and synergetic photo-chemotherapy. *Nanoscale*. 2019;11(43):20630–20637. doi:10.1039/C9NR06349H
24. Amani H, Mostafavi E, Arzaghi H, et al. Three-dimensional graphene foams: synthesis, properties, biocompatibility, biodegradability, and applications in tissue engineering. *ACS Biomater Sci Eng*. 2019;5(1):193–214. doi:10.1021/acsbiomaterials.8b00658
25. Chen XJ, Zhang MJ, Li SN, et al. Facile synthesis of polypyrrole@metal-organic framework core-shell nanocomposites for dual-mode imaging and synergistic chemo-photothermal therapy of cancer cells. *J Mater Chem B*. 2017;5(9):1772–1778. doi:10.1039/C6TB03218D
26. Li J, Zhang CT, Gong SM, et al. A nanoscale photothermal agent based on a metal-organic coordination polymer as a drug-loading framework for effective combination therapy. *Acta Biomater*. 2019;94:435–446. doi:10.1016/j.actbio.2019.06.014
27. Li SN, Zhang LY, Liang X, et al. Tailored synthesis of hollow MOF/polydopamine Janus nanoparticles for synergistic multi-drug chemo-photothermal therapy. *Chem Eng J*. 2019;378:122175.
28. Han XX, Xu Y, Li YY, et al. An extendable star-like nanoplatform for functional and anatomical imaging-guided photothermal oncotherapy. *ACS Nano*. 2019;13(4):4379–4391. doi:10.1021/acsnano.8b09607
29. Amani H, Arzaghi H, Bayandori M, et al. Controlling cell behavior through the design of biomaterial surfaces: a focus on surface modification techniques. *Adv Mater Interfaces*. 2019;6(13). doi:10.1002/admi.201900572
30. Wang XY, Zhang JS, Wang YT, et al. Multi-responsive photothermal-chemotherapy with drug-loaded melanin-like nanoparticles for synergetic tumor ablation. *Biomaterials*. 2016;81:114–124. doi:10.1016/j.biomaterials.2015.11.037
31. Zeng XW, Luo MM, Liu G, et al. Polydopamine-modified black phosphorous nanocapsule with enhanced stability and photothermal performance for tumor multimodal treatments. *Adv Sci*. 2018;5(10):201800510. doi:10.1002/advs.201800510
32. Dong ZL, Gong H, Gao M, et al. Polydopamine nanoparticles as a versatile molecular loading platform to enable imaging-guided cancer combination therapy. *Theranostics*. 2016;6(7):1031–1042. doi:10.7150/thno.14431
33. Hu DH, Zhang JN, Gao GH, Sheng ZH, Cui HD, Cai LT. Indocyanine green-loaded polydopamine-reduced graphene oxide nanocomposites with amplifying photoacoustic and photothermal effects for cancer theranostics. *Theranostics*. 2016;6(7):1043–1052. doi:10.7150/thno.14566
34. Liu XS, Cao JM, Li H, et al. Mussel-inspired polydopamine: a biocompatible and ultrastable coating for nanoparticles in vivo. *ACS Nano*. 2013;7(10):9384–9395. doi:10.1021/nn404117j
35. Miao ZH, Wang H, Yang HJ, Li ZL, Zhen L, Xu CY. Intrinsically Mn2+-chelated polydopamine nanoparticles for simultaneous magnetic resonance imaging and photothermal ablation of cancer cells. *ACS Appl Mater Inter*. 2015;7(31):16946–16952. doi:10.1021/acsami.5b06265
36. Zhao H, Chao Y, Liu JJ, et al. Polydopamine coated single-walled carbon nanotubes as a versatile platform with radionuclide labeling for multimodal tumor imaging and therapy. *Theranostics*. 2016;6(11):1833–1843. doi:10.7150/thno.16047
37. Dai Y, Yang DP, Yu DP, et al. Mussel-inspired polydopamine-coated lanthanide nanoparticles for NIR-II/CT dual imaging and photothermal therapy. *ACS Appl Mater Inter*. 2017;9(32):26674–26683. doi:10.1021/acsami.7b06109
38. Xing YX, Zhang JX, Chen F, Liu JJ, Cai KY. Mesoporous polydopamine nanoparticles with co-delivery function for overcoming multidrug resistance via synergistic chemo-photothermal therapy. *Nanoscale*. 2017;9(25):8781–8790. doi:10.1039/C7NR01857F
39. Zheng M, Liu S, Guan XG, Xie ZG. One-step synthesis of nanoscale zeolitic imidazolate frameworks with high curcumin loading for treatment of cervical cancer. *ACS Appl Mater Inter*. 2015;7(40):22181–22187. doi:10.1021/acsami.5b04315
40. Li MH, Sun XT, Zhang N, et al. NIR-activated polydopamine-coated carrier-free "nanobomb" for in situ on-demand drug release. *Adv Sci*. 2018;5(7):1800155. doi:10.1002/advs.201800155

41. Shao LH, Zhang RR, Lu JQ, Zhao CY, Deng XW, Wu Y. Mesoporous silica coated polydopamine functionalized reduced graphene oxide for synergistic targeted chemo-photothermal therapy. *ACS Appl Mater Inter*. 2017;9(2):1226–1236. doi:10.1021/acsami.6b11209
42. Liu C, Guo X, Ruan C, et al. An injectable thermosensitive photothermal-network hydrogel for near-infrared-triggered drug delivery and synergistic photothermal-chemotherapy. *Acta Biomater*. 2019;96:281–294. doi:10.1016/j.actbio.2019.07.024
43. Duan Y, Ye FG, Huang YL, Qin YM, He CM, Zhao SL. One-pot synthesis of a metal-organic framework-based drug carrier for intelligent glucose-responsive insulin delivery. *Chem Commun*. 2018;54(42):5377–5380. doi:10.1039/C8CC02708K
44. Chen L, Zhang JL, Zhou XJ, et al. Merging metal organic framework with hollow organosilica nanoparticles as a versatile nanoplatform for cancer theranostics. *Acta Biomater*. 2019;86:406–415. doi:10.1016/j.actbio.2019.01.005
45. Liu W, Zhang XY, Zhou L, Shang L, Su ZQ. Reduced graphene oxide (rGO) hybridized hydrogel as a near-infrared (NIR)/pH dual-responsive platform for combined chemo-photothermal therapy. *J Colloid Interface Sci*. 2019;536:160–170. doi:10.1016/j.jcis.2018.10.050